Available online at www.sciencedirect.com
ScienceDirect
Ceramics International 37 (2011) 1631–1636
CERAMICS INTERNATIONAL
www.elsevier.com/locate/ceramint

Electroconductive Alumina–TiC–Ni nanocomposites obtained by Spark Plasma Sintering

T. Rodriguez-Suarez [a,*], J.F. Bartolomé [b], A. Smirnov [b,c], S. Lopez-Esteban [a], L.A. Díaz [a], R. Torrecillas [a], J.S. Moya [b]

[a] *Centro de Investigación en Nanomateriales y Nanotecnología (CINN), Consejo Superior de Investigaciones Científicas (CSIC) - Universidad de Oviedo (UO) - Principado de Asturias (PA), Parque Tecnológico de Asturias, 33428 Llanera (Asturias), Spain*

[b] *Instituto de Ciencia de Materiales de Madrid (ICMM), Consejo Superior de Investigaciones Científicas (CSIC), C/Sor Juana Inés de la Cruz, 3, 28049 Cantoblanco (Madrid), Spain*

[c] *Department of Materials Engineering, Tallinn University of Technology, Ehitajate tee 5, 19086 Tallinn, Estonia*

Received 30 November 2010; received in revised form 27 December 2010; accepted 20 January 2011
Available online 18 February 2011

Abstract

In the present work, the processing and characterization of electroconductive Alumina–TiC–Ni nanocomposites obtained by Spark Plasma Sintering (SPS) are described. These nanocomposites are singular due to the excellent mechanical properties they present (particular regarding Vickers hardness, 25.6 ± 0.7 GPa), as well as their extremely good wear behaviour, studied under ''ball-on-disk'' dry sliding conditions. The wear rate obtained was 25 times (almost 1.5 orders of magnitude) smaller than the value obtained for a monolithic alumina sintered under the same conditions. Flexural strength had been improved up to 75% with respect to the monolithic alumina processed under the same conditions. As these nanocomposites can be machined by electroerosion (EDM), they can adopt any shape for devices requiring a good mechanical performance and low wear rates.

Keywords: B. Nanocomposites; C. Mechanical properties; C. Wear resistance; Electroerosion

1. Introduction

Ceramic–metal nanocomposites are of great interest due to the singularity they present: by the inclusion of secondary metallic phases in an appropriate content (below the percolation and aggregation threshold), particle grain size is limited to the nanoscale and matrix hardness can be improved. It has been showed that diamond-like hardening can be obtained by the addition of a second metallic nanometric phase to an also nanometric ceramic matrix obtaining better results when it is also comprised at the nanometric range [1–3].

The particular case of ceramic–nNi system has been widely studied. Zirconia–Ni and Alumina–Ni nanocomposites give maximum hardness values for a 2.5 vol.% Ni content [2,4]. Hardness was clearly improved in the case of alumina matrix nanocomposites reaching an H_V of 25 GPa for the latter composition [2]. One factor contributing to this high hardness value was nanostructure retaining by employing the Spark Plasma Sintering (SPS) for nanocomposites consolidation, which is a rapid solidification technique where high quality and uniform compacts can be sintered rapidly at comparatively lower temperatures when compared to conventional sintering methods. The main advantages of SPS process include (i) nanostructures preservation, (ii) the significant reduction in consolidation times and rapid densification of powders due to the synergetic combination of electrical energy and mechanical pressure and (iii) the maintenance of the novel properties of initial powder promoting the cost-effective fabrication of bulk nanocomposites [5].

The remarkably hardness improvement obtained by the authors on the Alumina–Ni system, makes these compositions difficult to machining to fulfil specific shapes by conventional techniques; hence their final cost will be increased and it use limited in some applications.

* Corresponding author at: Centro de Investigación en Nanomateriales y Nanotecnología (CINN), Consejo Superior de Investigaciones Científicas (CSIC) - Universidad de Oviedo (UO) - Principado de Astuiras (PA), Edificio Fundación ITMA, Parque Tecnológico de Asturias, 33428 Llanera (Asturias), Spain. Tel.: +34 985 98 00 58; fax: +34 985 26 55 74.
E-mail address: t.rodriguez@cinn.es (T. Rodriguez-Suarez).

0272-8842/$36.00
doi:10.1016/j.ceramint.2011.01.033

Alternatively, other machining methods independent on mechanical contact have been developed, as it is the case of EDM (Electro Discharge Machining), that is a nonconventional way of machining that has currently positioned as one of the most important techniques for machining hard materials for industrial applications and has become an integral part for making prototypes since it avoids using expensive grinding operations for final shaping and surface finishing of components [6]. Because the conventional grinding techniques involve costly synthetic diamonds and long period of machining, the electroerosion technique provides some advantages such as favourable production costs, high precision, versatility and degree of automation [7].

The EDM wire technology opens up new opportunities for ultra-precise machining of miniaturized components in various fields of technology, including aerospace, defence, medical instruments, semiconductor that may require wire diameters down to 0.02 mm [8].

In comparison with conventional machining techniques, EDM achieves higher removal rates for these materials with respect of surface integrity and also tolerances of below 1 μm have been achieved with a high level of flexibility while reducing running cost. Materials electrical resistivity should be lower than 100–300 Ω cm for being electrical discharge machinable [9]. In this sense, for making these ultrahard materials electrical conductors, a third semiconductor nanophase, over the percolation threshold, can be added. By this additional property induced to these materials, they become electrical conductors and, hence, electrical discharge machinable. The addition of a semiconductor phase to a ceramic–metal system has been successfully processed in the zirconia–Ni system [9].

These superhard materials find applications such as bearings, different purpose cutting tools (for turning and boring operations as roughing and finishing of several alloys and steels), nozzles for inkjet tile and dinnerware decoration, electrodes, high wear resistance brakes, electronic devices, etc.

In this regard, the study of superhard materials has received increasing attention from the scientific, technical and practical points of view. In the present investigation efforts have been devoted to develop superhard and wear resistant materials based on the singular properties of nanoparticles.

2. Experimental procedure

2.1. Starting materials

The following commercial available powders have been used: (i) alumina powder (α-alumina (99.99%, Taimei Chemical Co., Ltd., Japan) with an average particle size of $d_{50} = 250 \pm 50$ nm), (ii) Nickel (II) nitrate hexahydrate (Merck, Germany, 99.0% purity, ($Ni(NO_3)_2{\cdot}6H_2O$)) and (iii) Titanium Carbide (Hubei Minmetals) with an average particle size of $d_{50} \approx 20$ nm.

2.2. Processing of Alumina–TiC–Ni nanocomposites

Nickel (II) nitrate hexahydrate was weighed in order to have the desired metal volume content in the final composites and was initially completely dissolved in alcohol by ultrasonic agitation. Subsequently, alumina powder was mixed with this alcoholic solution and ball milled for 24 h with Al_2O_3 balls. The mixture was dried at 120 °C, ground in an agate mortar and then calcined at 400 °C for 2 h in air to obtain Al_2O_3/NiO mixed powders. Subsequently, the powders were sieved down 32 μm. Composition of 2.5 vol.% was selected for giving highest hardness values [2].

These Al_2O_3/NiO powders were mixed with TiC nanopowders in distilled water media. TiC content was selected to be 25 vol.% (with respect to the final composition) for being a concentration over the percolation threshold ($f_c \sim 16$ vol.%). Rheological parameters were fixed as 50% solids load with the addition of 4 w% of a deffloculant, dolapix CE-64. Suspensions were homogenized in polyethylene containers with zirconia balls for 2 h. Then, suspensions were dried in a furnace at 100 °C. Dried powders were sieved again under 32 μm and reduced at 500 °C for 2 h under a 90%Ar/10%H_2 atmosphere, giving final Alumina–TiC–Ni nanopowders. The selected composition was 75 vol.% of (Alumina + 2.5 vol.% nNi) and 25 vol.% nTiC, hence, final concentrations were 73.1 vol.% Alumina + 1.9 vol.% nNi + 25 vol.% nTiC.

2.3. Spark Plasma Sintering

The compaction the obtained powders was performed by SPS (FCT Systeme GMBH, HPD25, Germany). Cylindrical samples with a diameter of 20 and 40 mm and height of 2–4 mm were prepared as follows; (i) the sample were heated from room temperature to 600 °C at a rate of 600 °C/min, using a pressure of ∼10 MPa; (ii) from 600 °C to 1100 °C a heating rate of 200 °C/min and a pressure of ∼10 MPa was used; (iii) from 1100 °C to 1375 °C a heating rate of 50 °C/min and pressure of 100 MPa was used and these final temperature and pressure were maintained for 3 min. In terms of comparison, alumina powders were SPSed too following the latter sintering cycle.

2.4. Characterization

The microstructure of sintered specimens was studied on fracture surfaces by Scanning Electron Microscopy (FE-SEM, FEI Nova NANOSEM 230, Oregon, USA and Zeiss Ultraplus, Germany). Alumina–TiC–Ni nanocomposites were also studied in a transmission electron microscopy TEM (Jeol microscope, model FXII, JEM 2000, Japan, operating at 200 kV).

The Vickers hardness, H_V, of the SPSed samples was determined by microindentation (Buehler model Micromet 5103, Germany) on sample surfaces polished down to 1 μm, applying a 1.96 N load with an indentation time of 10 s. The magnitude of the Vickers hardness was determined according to,

$$H_V = 1.854\frac{P}{d^2} \quad (1)$$

where P is the applied load (in N) and d is the diagonal length (in m).

The toughness, K_{IC}, was also determined by microindentation (diamond indenter Leco 100-A, St. Joseph, MI, USA), but, for this specific property, the applied load was 98 N with an indentation time of 10 s. The fracture toughness was calculated using the formula given by Miranzo and Moya [10].

The flexural strength, σ_f, was evaluated at room temperature by a three point bending test in a SHIMADZU (AutoGraph AG-X, Japan) 5 kN universal testing machine using prismatic bars cut from the pieces previously fired with 4 mm width, 30 mm length and 3 mm thickness being the span 20 mm. The tensile surfaces were polished down to 1 μm and specimens were loaded to failure with a crosshead speed of 0.5 mm/min.

Finally, the electrical resistance of Alumina–TiC–Ni nanocomposites was measured with a four-wire (Kelvin) connection method using a separate current source (Keithley 6220, Cleveland, OH, USA) and a two-channel nanovoltmeter (Keithley 2182A, Cleveland, OH, USA).

2.5. Wire-electroerosion machining (EDM)

Wire-cutting EDM uses a metallic wire to cut a programmed contour in a workpiece. Metallic wire and workpiece are both electrodes, separated by a dielectric liquid and subject to an electric voltage [9]. The wire can be inclined, making it possible to make parts with different profiles at the top and bottom. The wire is usually made of brass or stratified copper and between 0.02 and 0.3 mm has a diameter. When the distance between electrodes is reduced, a discharge flows between the two electrodes. Once the discharge starts, plasma is formed in the neighbourhood of the machined front [9].

For EDM purposes, one of the most advanced technology electroerosion machine has been employed (Agie SA - Agiecut Agievison 5, Switzerland), which avoids wire or electrode breakage. Cutting parameters are normally tabled by manufacturer and, in this particular case, parameters chosen were those corresponding to a hard metal as it is the case of tungsten carbide (WC) with negative polarity, implying more intensity than tension.

2.6. Tribological behaviour

A ''ball-on-disk'' type wear test was performed under ambient dry conditions in a Microtest tribometer (model MT/60/NI, Spain) in conformity with ASTM G99, using alumina balls and being the disks the materials tested. In this case, 3 mm diameter 99.9% pure alumina balls slid on the materials with a rotating speed of 3 rps and a radius of 0.8 mm. The applied load (F_N) was 10 N (corresponding to initial Hertzian contact pressures of 2.5 GPa) and tests lasted 60 h, which corresponded to a sliding distance (S) of ~3255 m. Before each test, the specimens and balls were rinsed ultrasonically in acetone. After each sliding test, the worn surfaces were cleared by blowing pressurized air before post-mortem observations. All tests were performed under the same conditions. Archimedes densities (ρ) in water were measured for all materials.

The wear rate was calculated by using Eq. (2):

$$W = \frac{\Delta V}{F_N S} \tag{2}$$

Being ΔV the volume loss after the tests (mm^3), F_N the applied load (N) and S the sliding distance (m). In order to estimate the volume losses correctly, the track profiles were analyzed with a 3D surface profilometer (Taylor-Hobson Talysurf, UK) which maps the surface morphology by putting a stylus in mechanical contact with the sample, being the step 0.01 μm and the scanning speed 0.1 mm/s. Profilometer was used to determine three dimensional surface topographic maps.

3. Results and discussion

3.1. Microstructural characterization

Fracture surfaces of materials case of study were analyzed by SEM. As can be clearly observed in Fig. 1, a significant microstructural refinement (smaller alumina matrix grains) occurs in Alumina–TiC–Ni nanocomposites. This is related, on one hand to the pinning effect held by Ni and TiC nanoparticles and, on the other hand, to the nanostructured features of powders preserved by employing SPS as sintering technique.

Fig. 1(a) and (b) shows that both materials present, mainly, an intergranular fracture. The mean alumina grain size is around 0.3 ± 0.1 μm in the ternary nanocomposite while in the

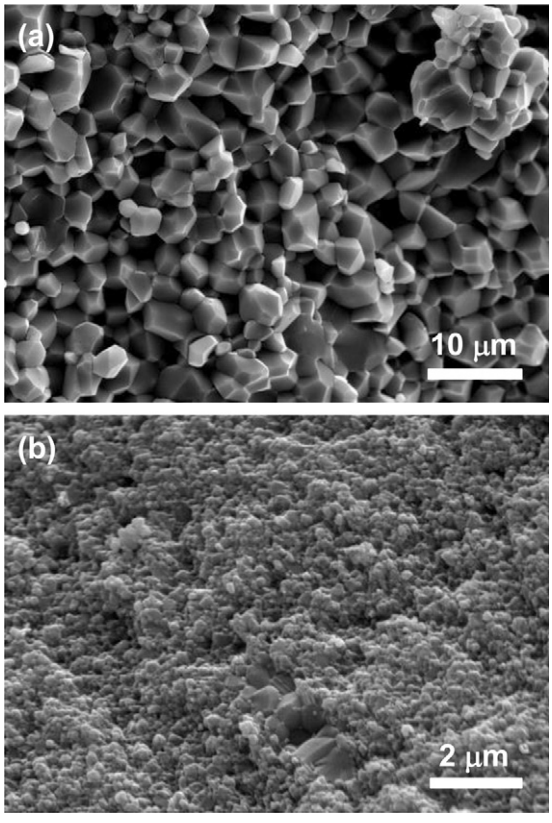

Fig. 1. SEM images corresponding to fracture surfaces of (a) Alumina and (b) Alumina–TiC–Ni nanocomposite.

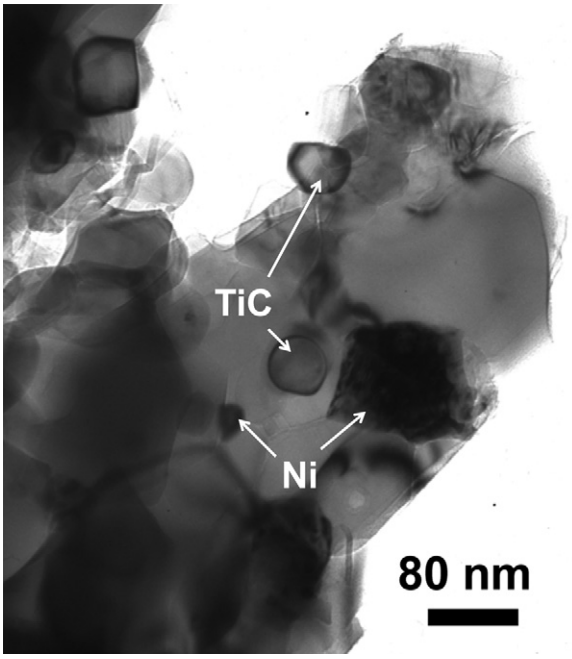

Fig. 2. TEM micrograph corresponding to SPSed Alumina–TiC–Ni nanocomposite.

monolithic material is 3 ± 1 μm. In the nanocomposite, the presence of small aggregates (<1 μm) is also observed.

The ternary nanocomposite nanostructure was studied, in more detail, by TEM (Fig. 2). In this figure Ni and TiC nanoparticles are observed. Although sintering at 1375 °C, nanoparticles have not significantly grown and the hardening effect obtained by Ni nanoparticles is, in this nanocomposite, expected.

The measured relative densities of sintered materials were found to be >98% th.

3.2. Mechanical properties: Vickers hardness, toughness and flexural strength

Evaluation of Vickers hardness (H_V), toughness (K_{IC}) and flexural strength (σ_f), together with densities measured are given in Table 1, where Alumina–TiC–Ni nanocomposite is shortly referred as AlNiTiC.

Vickers hardness for the nanocomposite has raised approximately 30% in comparison to monolithic alumina sintered under the same conditions. This fact can be explained in terms of the hardening effect held not only by Ni nanoparticles but also by TiC nanoparticles.

Table 1
Mechanical properties and densities corresponding to the materials studied.

	Al_2O_3	AlNiTiC
Vickers hardness H_V (GPa)	19.9 ± 0.9	25.6 ± 0.7
Toughness K_{IC} (MPa $m^{1/2}$)	3.5 ± 0.1	3.7 ± 0.1
Flexural strength σ_f (MPa)	395 ± 36	537 ± 88
Density ρ (g/cm^3)	3.93 ± 0.01	4.27 ± 0.01

Between the alumina and the nanocomposite the difference in toughness is almost negligible. It is well known that TiC particles play an important role in improving fracture toughness (*R*-curve behaviour) in Alumina–TiC microcomposites [11,12]. In our particular case, TiC particles are <2 μm, which is the critical size for fracture toughness improvement [13], so toughness values similar to the one of the alumina were expected.

At last, a significant improvement (about 75%), but has been achieved by the inclusion of Ni and TiC nanoparticles to the alumina matrix. This can be explained in terms of microstructural refinement, that is, smaller grain sizes (and so flaw sizes) give higher flexural strength values. Second phases size is not large enough for inducing any reinforcement, as it is deduced from toughness values.

3.3. Electrical conductivity of Alumina–TiC–Ni nanocomposites

The electrical resistivity (measured by four-wire ohmmeter) of Alumina–TiC–Ni nanocomposites with a semiconductor content above the percolation threshold, was found to be $3.15 \times 10^{-5} \pm 0.1\ \Omega$ m. This value is about 7 orders of magnitude lower than the limit of 1–3 Ω m, which make the material suitable for EDM.

3.4. EDM results

Workpieces were machined in a prismatic shape of 2.54 cm length and 7 mm height. Corners were curved ($R = 12.7$ mm) and 11° chamfers were also made in top and bottom sides, as it is shown in Fig. 3.

Surface finishing after electroerosion was analyzed in detail by FE-SEM. Fig. 4 shows the effects of the wire over the material surface after cutting. In this figure, two different process zones are observed. On one hand, there are places where the wire has caused materials fusion. This fused layer is between 0.5 and 1.5 μm depth. And, on the other hand, there are zones where nanostructure is still observed. In general terms, the final roughness of the workpiece after cutting is less than 1 μm.

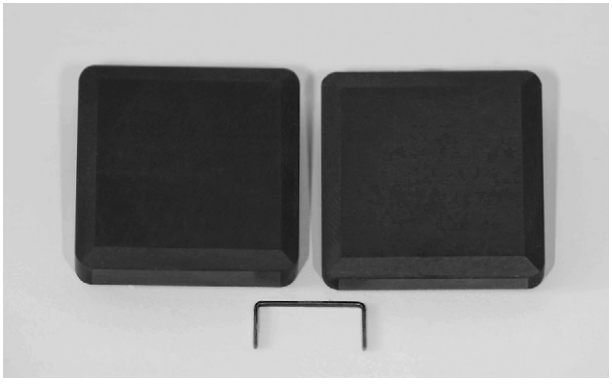

Fig. 3. Image showing final geometry of Alumina–TiC–Ni workpieces after electroerosion process.

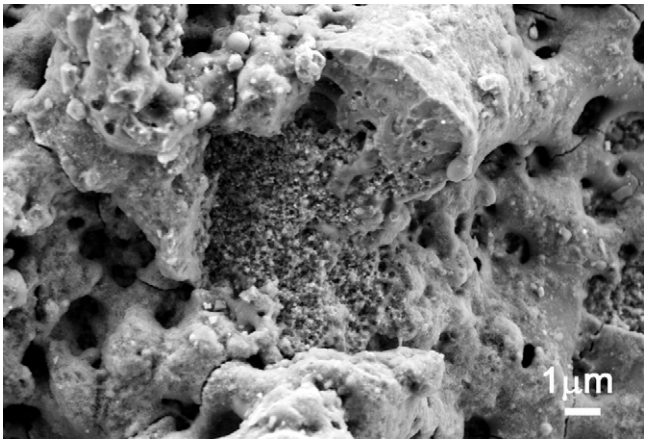

Fig. 4. FE-SEM micrograph showing Alumina–TiC–Ni surface finishing after EDM process.

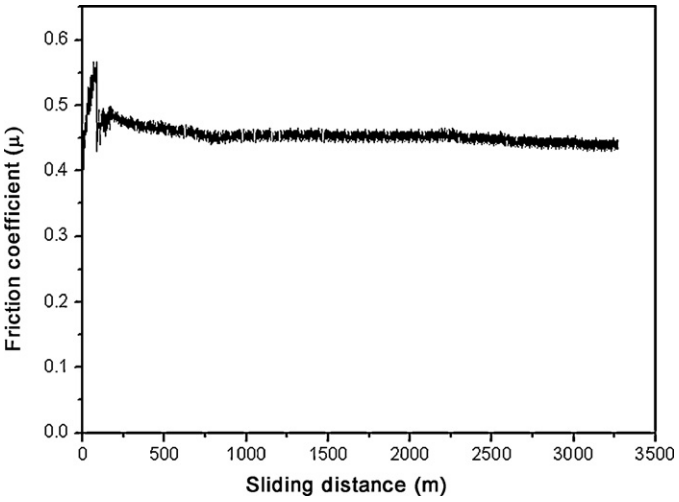

Fig. 5. Friction coefficient as a function of sliding distance corresponding to Alumina–TiC–Ni nanocomposite when sliding at 0.02 m/s under a 10 N contact load against a alumina ball.

3.5. Tribological behaviour

The friction coefficient (μ) is an important factor for understanding tribological behaviour. Fig. 5 represents the friction coefficient, as a function of the sliding distance, registered during the wear test for the Alumina–TiC–Ni nanocomposite with a 10 N applied load. Both materials tested exhibited similar behaviour. The friction coefficient increases rapidly throughout the first meters of sliding and, subsequently, decreases. After this initial stage, the variations in the curves become smaller and the friction coefficient slightly increases during the remaining testing time. This behaviour can be attributed to a polishing process during wear testing, establishing a smooth wear track surface, by ploughing away the surface asperities or roughness peaks.

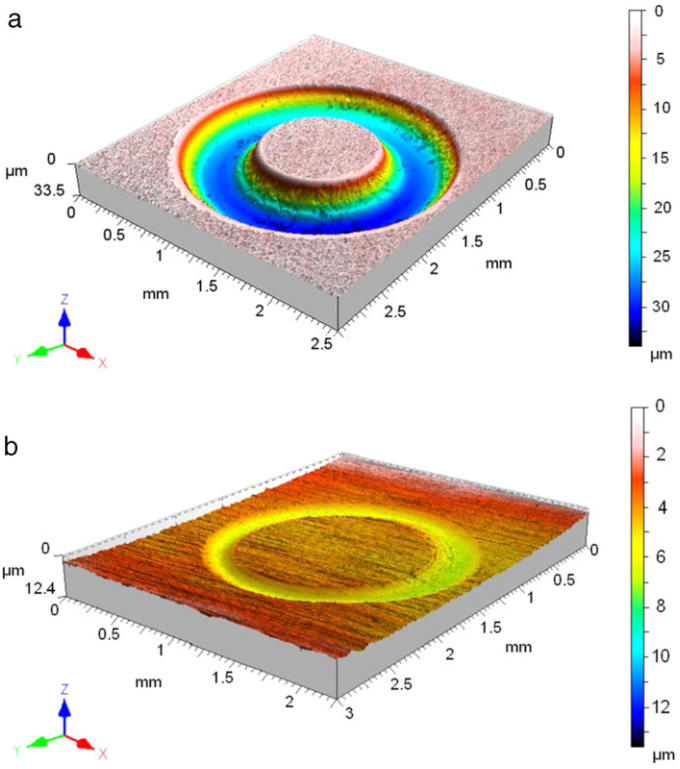

Fig. 6. 3D wear track topographies of (a) Al_2O_3 and (b) Alumina–TiC–Ni nanocomposite after "ball-on-disk" wear test against pure alumina balls (S = 3.25 km, F_N = 10 N, V = 0.02 m/s).

As the wear proceeds further, the wear track becomes smoother and the coefficient of friction fixes on a steady level. This polishing mechanism is exemplified in Table 2, in which the *Ra* and *Rt* surface roughness before and after wear tests are compared for samples and various sliding wear tracks. It is obvious that the roughness diminishes strongly during the first meters of sliding, and thus, the polishing effect is found to occur particularly within the running-in stage of the wear process.

The 3D wear track surface topographies corresponding to the materials after sliding against pure alumina ball are presented in Fig. 6. From the 3D wear track surface topographies, the corresponding wear track dimensions, i.e. depth and width, as well as the wear volume (W), were extracted for the all composition, as summarized in Table 3. Under identical conditions of sliding radio, sliding speed and contact load, the smallest depth and width of the wear tracks were measured for the Alumina–TiC–Ni nanocomposite.

Table 2
Materials surface roughness, *Ra* and *Rt*, as a function of sliding distance (S) when sliding at 0.02 m/s against alumina balls under a 10 N contact load.

S (km)	*Ra* (μm)				*Rt* (μm)				Friction coefficient (μ)
	0	0.1	1.5	3.25	0	0.1	1.5	3.25	
Al_2O_3	0.69	0.53	0.39	0.19	1.33	0.99	0.37	0.31	0.40
AlNiTiC	0.40	0.32	0.17	0.13	1.18	0.79	0.39	0.33	0.39

Table 3
Wear track dimensions and wear rates (W) corresponding to the materials essayed after "ball-on-disk" wear tests against pure alumina balls (S = 3.25 km, $v = 0.02$ m/s, F_N = 10 N).

Material	Width (μm)	Depth (μm)	W (mm^3/N m)
Al_2O_3	598	27.6	6.8×10^{-6}
AlNiTiC	269	4.3	2.7×10^{-7}

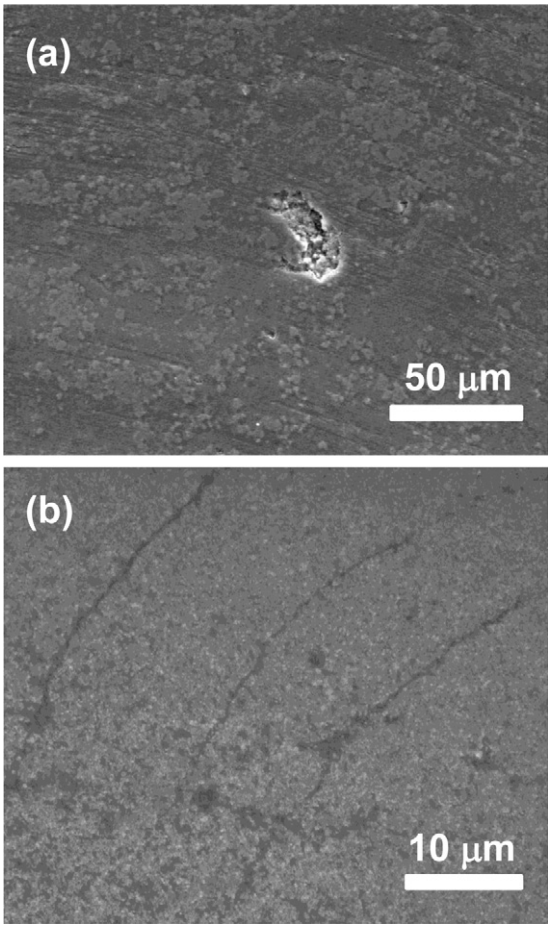

Fig. 7. SEM micrographs corresponding to the worn surfaces of (a) Al_2O_3 and (b) Alumina–TiC–Ni nanocomposite.

Further examinations of the materials wear surfaces confirmed that the observed changes in wear rate behaviour related to a fundamental change in process of wear. The monolithic alumina worn surface was generally rough (Fig. 7(a)). Occasional evidence of pull out was observed. This morphology is generated by an intragranular fracture dominated material removal mechanism. Fig. 7(b) shows a SEM micrograph of the worn surface of the nanocomposite generated under the same sliding conditions. A relatively smooth region is observed. In this material, no microcrack or microfracture is found at the contact surface.

The difference in the wear resistance between alumina and Alumina–TiC–Ni nanocomposites under dry-sliding conditions depends on material hardness, and also on the refinement of the alumina grain size in the nanocomposite. Both parameters seem to be the most important for improving the tribological properties at the working conditions essayed.

4. Conclusions

The results obtained in the present investigation clearly point out that the Alumina–TiC–Ni nanocomposite materials obtained by Spark Plasma Sintering can be considered as excellent candidates for wear resistant components and, since they present the advantage of being electroerosion machinable, they could adopt any intricate shape making them optimal materials for giving solutions to many advanced industrial applications.

Acknowledgements

This work has been supported by the Spanish Ministry of Science and Innovation under MAT2009-14542-C02 Project and CSIC through PIE Projects 200860I118 and 200860I119. A. Smirnov has been supported by ITMA Foundation and CSIC by JAE Predoctoral Programme 2010.

References

[1] J.S. Moya, S. Lopez-Esteban, C. Pecharromán, The challenge of ceramic/metal microcomposites and nanocomposites, Prog. Mater. Sci. 52 (2007) 1017–1090.
[2] J.S. Moya, T. Rodriguez-Suarez, S. Lopez-Esteban, C. Pecharromán, R. Torrecillas, L.A. Díaz, M. Nygren, Diamond-like hardening of alumina/Ni nanocomposites, Adv. Eng. Mater. 9 (2007) 898–901.
[3] T. Rodriguez-Suarez, L.A. Díaz, R. Torrecillas, S. Lopez-Esteban, W.-H. Tuan, M. Nygren, J.S. Moya, Alumina/tungsten nanocomposites obtained by Spark Plasma Sintering, Compos. Sci. Technol. 69 (2009) 2467–2473.
[4] C. Pecharromán, F. Esteban-Betegón, J.F. Bartolomé, G. Richter, J.S. Moya, Theoretical model of hardening in zirconia–nickel nanoparticle composites, Nano Lett. 4 (2004) 747–751.
[5] V. Viswanathan, T. Laha, K. Balani, A. Agarwal, S. Seal, Challenges and advances in nanocomposite processing techniques, Mater. Sci. Eng. R 54 (2006) 121–185.
[6] B. Lauwers, J.P. Kruth, W. Liu, W. Eeraerts, B. Schacht, P. Bleys, Investigation of material removal mechanisms in EDM of composite ceramic materials, J. Mater. Process. Technol. 149 (2004) 347–352.
[7] V. Tabacaru, M. Banu, S. Bouvier, Machinability analysis by wire cut electroerosion of special hard metals, Nonconventional Tech. Rev. 2 (2007) 113–116.
[8] http://www.gfac.com/fileadmin/user_upload/dev-agiecharmilles/Products/EDM/DS_EDM/EDM_Product_Range_EN_Oct2009.pdf (03/11/2010).
[9] S. Lopez-Esteban, C.F. Gutierrez-Gonzalez, G. Mata-Osoro, C. Pecharroman, L.A. Diaz, R. Torrecillas, J.S. Moya, Electrical discharge machining of ceramic/semiconductor/metal nanocomposites, Scripta Mater. 63 (2010) 219–222.
[10] P. Miranzo, J.S. Moya, Elastic/plastic indentation in ceramics: a fracture toughness determination method, Ceram. Int. 10 (1984) 147–152.
[11] J. Gong, Z. Zhao, H. Miao, Z. Guan, R-Curve behavior of TiC particle reinforced Al_2O_3 composites, Scripta Mater. 43 (2000) 27–31.
[12] J. Gong, Z. Zhao, Z. Guan, On the local crack resistance of Al_2O_3–TiC composites evaluated by direct indentation method, J. Eur. Ceram. Soc. 21 (2001) 941–946.
[13] J. Gong, H. Miao, Z. Zhao, The influence of TiC-particle-size on the fracture toughness of Al_2O_3–30 wt.%TiC composites, J. Eur. Ceram. Soc. 21 (2001) 2377–2381.